

液-液雾化的射流特性与粒径分布

梁坤峰, 彭正标, 袁竹林, 凡凤仙

(东南大学 能源与环境学院, 江苏 南京 210096)

摘 要: 液滴的粒径分布是液-液循环流化床制取流体冰技术的关键因素之一。在流化床实验装置上, 采用快速摄像与图像处理相结合的方法, 研究低流速下液-液单孔雾化的射流及其对液滴粒径分布的影响, 射流长度的变化和液滴的粒径分布运用数学统计的方法进行分析。研究结果发现, 当射流速度大于 1.14 m/s 时, 开始出现射流; 各个流速工况下射流长度的波动具有随机和非周期的特点, 其均值与方差随射流速度增大的总体变化趋势是先增大后减小; 转折点在射流速度为 6.58 m/s 时, 在射流长度波动的峰点处形成球形或锥形射流顶部是液滴的粒径具有大小差异及其运动路径发生摆动的主要原因; 各流速工况下, 液滴的粒径分布与 Rosin-Rammler 分布符合的很好; 研究结果为液-液循环流化床实际运行时控制雾化形成液滴的粒径分布提供可靠依据。

关键词: 液-液循环流化床; 液-液雾化; 射流; 液滴; 粒径分布

中图分类号: TB657.1 文献标识码: A

引 言

流体冰是近年新发展起来的一种新冰种, 具有流动性、换热性能好和可用泵进行输送等优点, 在制冷空调、化工、医疗等用冷场合的应用前景非常广阔, 流体冰的制取与应用在制冰界引起广泛关注^[1~3]。液-液循环流化床是以制取流体冰为背景而提出的一种新型流化制冰技术^[2~3], 液-液雾化形成细小水滴增大了两种液体的接触表面积, 极大地强化了两相间的传热与传质过程, 该方法将具有高效传热传质能力的流化床技术引入制冰领域, 充分发挥了多相流动与传热的重要作用。流化床内液滴的粒径均匀性和尺寸大小是制取流体冰技术的重要影响因素, 对液-液雾化过程中形成水滴的粒径分布进行控制成为液-液循环流化床制取流体冰的一个关键问题。

液-液雾化形成液滴问题随着喷墨、纤维纺丝、混合、萃取与乳化等技术的发展, 已成为工业应用研究的热点问题之一。目前针对该问题进行的数值与实验研究, 主要集中在有限空间内液滴形成的基础问题^[4~8]。由于针对大空间内液滴形成问题的研究很少, 液滴的形成过程涉及到惯性力、粘性力、浮力与界面张力的相互作用, 问题非常复杂, 虽然有不少研究成果可供参考, 但对循环流化床内液-液雾化形成液滴过程的研究依然具有挑战性。

针对制取流体冰这种特殊的应用背景, 建立液-液循环流化床实验系统, 研究水在另一种互不相溶的液体中雾化形成水滴问题。本文运用数学统计方法对低流速下液-液单孔雾化过程中射流长度的变化规律及形成液滴的粒径分布进行研究, 探讨射流变化影响液滴粒径分布的机理。

1 实验研究

2.1 实验装置

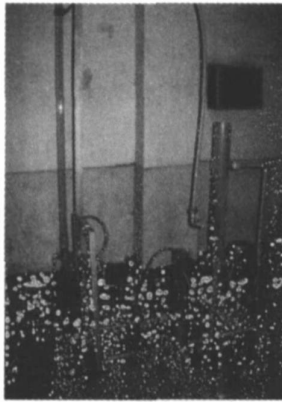
液-液循环流化床实验系统如图 1 所示, 实验装置的具体型号与结构参数可参考文献[9]。实验过程中, 实验流体分两路进入流化床, 一路为变压器油, 另一路为水(加入红色颜料, 增大对比度, 便于拍照)。变压器油首先由离心油泵(YG50-100), 油过滤器进入流化床, 采用齿轮流速计(LC-40)测量流速, 通过阀门将其调节到实验点, 流速为 0.18 m/s ; 待流动稳定之后, 打开增压泵(12WZ-8)抽取水箱的水, 水增压后从孔径为 0.22 mm 的喷头直接喷入床内, 射流速度由玻璃转子流速计(LZJ-10)读取, 用阀门将流速调节到实验点时, 打开采光室上部的强光源, 光线通过透光口将床内液滴形成过程反射到数码相机, 数码相机以 30 f/s 的频率进行连续拍

收稿日期: 2006-10-16; 修订日期: 2006-12-06

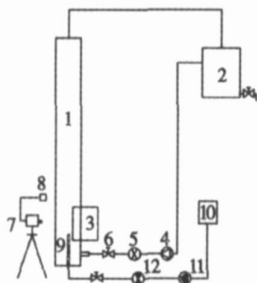
基金项目: 教育部高等学校博士点专项科研基金资助项目(20060286034)

作者简介: 梁坤峰(1975-)男, 河南新郑人, 河南科技大学讲师, 博士研究生。

摄,分别改变水的体积流量为 2.6, 4.4, 5.7, 6.2, 10, 15 和 20 mL/min, 获得距离喷孔 0~50 mm 高度内不同流速工况下的液滴形成过程的 100 幅照片。



(a) 试验装置



1-流化床;2-油水分离器;3-采光室;4-离心油泵;
5-齿轮流量计;6-阀门;7-数码CCD;8-强光源;
9-喷头;10-水箱;11-增压泵;12-玻璃转子流量计

(b) 试验系统

图1 液-液循环流化床实验系统

1.2 液-液单孔雾化现象

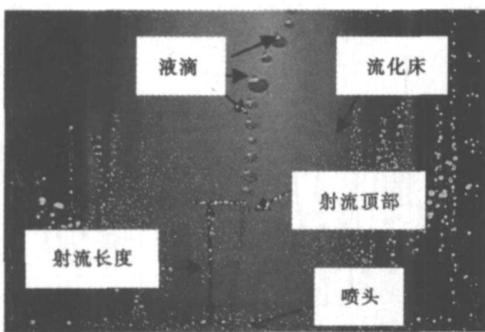


图2 液-液单孔雾化示意图

图2为低流速下液-液单孔雾化过程形成液滴的示意图。由图可知,水从喷孔处喷入充满变压器

油的流化床内,在喷孔上方会形成一个连续的射流,在周围流动变压器油的作用下,射流上部发生破碎形成一个个水滴(后文统一用液滴),射流的连续不破碎的高度称作射流长度,不发生破碎的射流最高点用射流顶部表示,不同的实验工况下,射流长度的高低不断变化,射流顶部的形状也在不断变化,所形成液滴的球形度较好,但其粒径大小并不一致,形成液滴的粒径存在均匀性问题,具有一定的分布特征。

2 实验结果与分析

进行了7个实验流量工况,其射流速度(射流在喷口处的平均流速)分别为 1.14, 1.93, 2.5, 2.72, 4.39, 6.58 和 8.77 m/s。由文献[9]可知,当射流速度大于 1.14 m/s 时,出现连续的射流,即射流长度不为零,且在同一工况的不同时刻,液滴形成的位置和粒径大小均动态变化。为了定量研究液-液雾化过程的射流及其破碎形成液滴的粒径随射流速度的变化特征,需要得到不同流速工况下的射流长度以及形成液滴的粒径信息。本文采取图像处理的方法,将原始图像进行灰度处理,调整其灰度等级,提高图像的信噪比,经过处理的图像,射流顶部和液滴与环境的对比鲜明,在其边缘利用灰度差,进行边缘检测,可以对射流长度及液滴的粒径进行测量,具体的处理方法参考文献[9]。

2.1 射流特性

2.1.1 射流长度的变化规律

对拍摄 3 s 时间内的 90 幅照片,提取每一幅照片的射流长度值,测量结果绘制如图 3 所示。由图可知,随着时间的变化,各个流速工况下的射流长度呈现波动特征,波动的幅度忽大忽小,具有随机和非周期的特点。出现这种现象是因为一旦出现射流,即射流长度不为零,液滴就必然在一个流动的液体中形成,此时射流破碎的激励来自于水的惯性力,周围液体的粘性力,界面张力,两相界面的扰动等综合作用,因此射流破碎的时间和位置都是不确定的。

但从射流长度随时间变化的统计特征看,波动幅度有一个均值,射流长度在均值上下进行波动,当射流速度分别为 1.93、2.5、2.72、4.39、6.58 和 8.77 m/s 时,射流长度波动的均值分别为 2.9、4.8、2.72、21.1、28 和 17.2 mm,表明随射流速度的增大,射流长度波动均值的总体变化趋势是先增大后减小,其最大值出现在射流速度为 6.58 m/s;同时在相同的射流速度工况下,射流长度波动的方差分别是 1.5、3.3、4.9、16.4、19.2 和 6.4,由于方差是用来度量数

据的分散程度, 由此可知在射流速度位于 4.39 ~ 6.58 m/s 之间时, 射流长度波动的幅度, 即射流的破碎长度要远大于其它流速; 另外, 对射流长度波动曲线进行两次多项式拟和, 得到其波动趋势线, 如图中实线所示, 发现在射流速度为 6.58 m/s 时, 其波动

趋势线为曲线, 其它流速工况下的波动趋势线均为直线; 从波动趋势线的变化规律看, 射流长度波动的转折点是射流速度为 6.58 m/s 时, 此时射流处于最不稳定的状态。

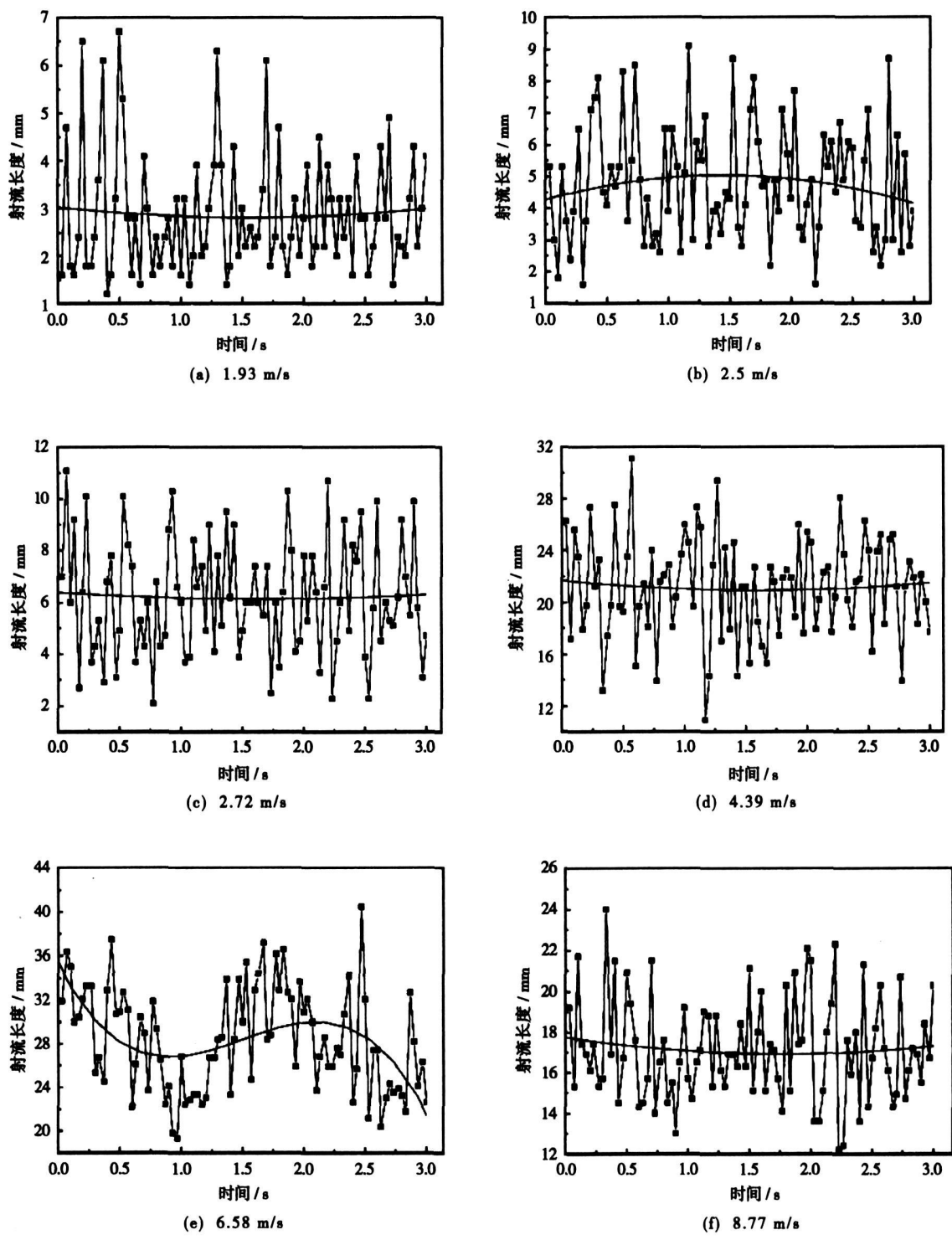


图 3 不同流速工况下的射流长度

2.1.2 射流顶部的变化规律

每个流速工况下1 s内射流长度波动的7个峰点与谷点对应的雾化照片,如图4所示。图中上下两组图片分别对应射流长度波动的峰点与谷点。由图可知,在射流速度分别为1.93、2.5、2.72和4.39 m/s时,由于射流长度波动的峰点处于射流发展的最高点,受周围液体的粘性力和自身重力作用,与处于谷点处的射流相比会形成较大的球形或锥形射流顶部,此时射流自身的惯性力与周围液体的曳力不

足以维持其沿着从喷孔射出时的直线方向运动,运动方向发生弯曲;当射流从最不稳定的顶部开始破碎,即射流长度从峰点向谷点发展时,形成的液滴必然具有大小差异,表现一定的分布特征,其运动路径也会由于射流的运动方向发生弯曲而摆动。随着流速的变化,峰点处形成的球形或锥形射流顶部以及射流长度增大,导致射流的破碎长度与射流方向的弯曲程度增加,从而使形成液滴的粒径分散度(不均匀性)及其运动路径的摆动也增大。



图4 射流长度波动的峰点与谷点对应的雾化照片

当射流速度增大到6.58 m/s时,界面处液-液两相较大的速度差,加强了周围液体的扰动作用,使射流的破碎长度增加,处于峰点的射流较难形成较

大的射流顶部,此时射流破碎形成的液滴粒径均匀性得到改善,其运动路径的摆动主要是受周围液体流动的影响。随着射流速度的继续增大,界面处两

相的速度差增大,在射流自身惯性与周围液体扰动的共同作用下,难以形成较大的射流顶部,射流最开始破碎的位置下移,此时液滴的粒径均匀性较好,其运动路径的摆动明显减弱。

2.2 液滴的粒径分布

通常,液滴的粒径分布常用数学函数法进行表示,较为常用的有正态分布函数、对数分布函数、Rosin-Rammler 分布函数等,经过对几种分布函数的比较分析,发现流化床内液-液雾化形成液滴的粒径分布与 Rosin-Rammler 分布具有较好的一致性。

Rosin-Rammler 分布表达式为^[10]:

$$F(d) = \exp[-(d/\bar{d})^m] \tag{1}$$

式中: $F(d)$ —分布函数,其值为筛上累计质量分数;
 d —液滴粒径; \bar{d} —液滴粒径的特征尺寸,取 $F(d)=$

$e^{-1} \approx 0.368$ 时的粒径值; m —分布参数,又称均匀性系数,表征液滴的粒径分布的分散度。

将式(1)改写成:

$$\ln(-\ln F(d)) = m \cdot \ln d - m \cdot \ln \bar{d}$$

或 $m = \frac{\ln(-\ln F(d))}{\ln d - \ln \bar{d}}$ (2)

式(2)表明,如果液滴的粒径分布符合 Rosin-Rammler 分布函数时,在双对数 $\ln(d)$ 与 $\ln(-\ln F(d))$ 坐标系下,所绘制的粒径分布曲线的回归曲线应为一 条直线,直线的斜率为 m 。

对实验流速范围内的 7 个工况,采用图像处理方法进行液滴粒径的测量,每个工况取 100 个液滴,获得雾化过程形成液滴的粒径信息。根据液滴的粒径信息,计算 7 个流速工况下,各粒径范围对应的筛上累计质量分数,如表 1 所示。

表 1 液滴的筛上累计质量分布

射流速度/ $m \cdot s^{-1}$													
1.14		1.93		2.5		2.72		4.39		6.58		8.77	
d/mm	$F(d)/\%$	d/mm	$F(d)/\%$	d/mm	$F(d)/\%$	d/mm	$F(d)/\%$	d/mm	$F(d)/\%$	d/mm	$F(d)/\%$	d/mm	$F(d)/\%$
1.63	0.952	1.48	0.955	1.21	0.929	0.95	0.965	0.85	0.969	1.11	0.909	0.94	0.974
1.83	0.900	1.85	0.841	1.51	0.815	1.31	0.832	1.11	0.922	1.41	0.751	1.31	0.596
2.05	0.724	2.21	0.482	1.95	0.552	1.88	0.468	1.68	0.685	1.85	0.327	1.57	0.345
2.25	0.537	2.41	0.285	2.23	0.342	2.11	0.314	2.41	0.360	2.04	0.157	1.75	0.182
2.55	0.232	2.51	0.139	2.38	0.146	2.28	0.177	2.88	0.083	2.26	0.042	2.01	0.040
2.64	0.000	2.64	0.000	2.45	0.000	2.43	0.000	3.02	0.000	2.37	0.000	2.07	0.000

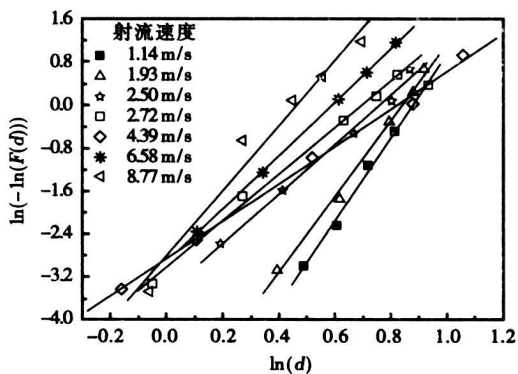


图 5 双对数坐标下 Rosin-Rammler 分布函数关系曲线

根据 Rosin-Rammler 分布函数的要求,由式(2)以及表 1 中的数据,可以得到不同流速下,用该分布表示的液滴粒径分布散点图及回归曲线,如图 5 所示。液滴的粒径分布与 Rosin-Rammler 分布函数的

符合情况可以用回归曲线的相关系数判断,由图 5 中不同射流速度下粒径分布的回归直线及表 2 中回归直线的相关系数可知,不同流速工况下回归直线的线性回归良好,能很好的符合 Rosin-Rammler 分布函数。

表 2 回归直线的相关系数

射流速度/ $m \cdot s^{-1}$	相关系数
1.14	0.995 2
1.93	0.994 7
2.5	0.992 5
2.72	0.996 3
4.39	0.996 4
6.58	0.999 4
8.77	0.967 1

3 结 论

本文针对液-液循环流化床制取流体冰方法的一项关键技术—液-液雾化展开实验研究并获得以下结论:

(1) 在同一工况的不同时刻, 液-液雾化过程中形成液滴的位置和粒径大小是动态变化的, 其射流长度的波动表现出随机的和非周期的特点。

(2) 随着射流速度的增大, 射流长度波动的均值与方差的总体变化趋势是先增大后减小的, 最大值均出现在射流速度为 6.58 m/s 时, 表明该射流速度是射流长度的增长变化与波动的转折点。

(3) 在射流长度的峰点处形成球形或锥形射流顶部, 当射流长度从峰点向谷点发展时, 射流破碎形成的液滴粒径具有大小差异, 其运动路径也由于射流的运动方向发生弯曲而摆动。

(4) 各流速工况下, 液滴粒径分布与 Rosin-Rammler 分布符合的很好, 可以采用该分布函数对液滴的粒径分布进行研究。

参考文献:

[1] AKIO SAITO. Recent advances in research on cold thermal energy storage[J]. International Journal of Refrigeration, 2002, 25(2): 177-189.

- [2] 袁竹林. 制取流体冰新方法及高效冰蓄冷研究[J]. 能源研究与利用, 2004(4): 36-40.
- [3] 梁坤峰, 彭正标, 袁竹林. 液-液循环流化床制冰过程的分析[J]. 东南大学学报, 2006, 36(5): 774-779.
- [4] RICHARD JOHN R, BERIS ANTONY N, LENHOFF ABRAHAM M. Steady laminar flow of liquid-liquid jets at high Reynolds numbers[J]. Physics of Fluids, 1993, A5(7): 1703-1717.
- [5] RICHARDS J R, LENHOFF ABRAHAM M, BERIS ANTONY N. Dynamic breakup of liquid-liquid jets[J]. Physics of Fluids, 1994 6(8): 2640-2655.
- [6] RICHARDS J R, BERIS ANTONY N, LENHOFF ABRAHAM M. Drop formation in liquid-liquid systems before and after jetting[J]. Physics of Fluids, 1995, 7(11): 2617-2630.
- [7] ZHANG XIAO GUANG. Dynamics of drop formation in viscous flows[J]. Chemical Engineering Science, 1999, 54(12): 1759-1774.
- [8] CARSTEN CRAMER, PETER FISCHER, WINDHAB ERICH J. Drop formation in a co-flowing ambient fluid[J]. Chemical Engineering Science, 2004, 59(15): 3045-3058.
- [9] 梁坤峰, 袁竹林, 彭正标, 等. 液-液雾化特性与粒径分布规律[J]. 化工学报 2007(待发表).
- [10] MACIAS GARCIA A, CUERDA CORREA EDUAR DO M, DIAZ DIEZ MA. Application of the Rosin-Rammler and Gates-Gaudin-Schuhmann models to the particle size distribution analysis of agglomerated cork[J]. Materials Characterization, 2004, 52(2): 159-164.

(编辑 何静芳)

能源利用

燃用生物质燃料的 2.5 MW 工业燃气轮机

据《Gas Turbine World》2006 年 9—10 月号报道, 加拿大 Orenda 公司正在销售供商业营运、能用生物质燃料、乙醇和原油作为替代燃料的改型的 OGT2500 燃气轮机。

燃气轮机的修改包括高温部分的重新设计、雾化燃料喷射、适应性控制、高温部分在线清洗。

新的燃料处理模块具有用于燃料预热、混合、过滤、转输和燃料管线清洗的设备。

在 ISO 条件下, 用天然气作为燃料, OGT2500 基本负荷的额定输出为 2670 kW, 热耗率为 13 483 kJ/(kWh) (热效率为 26.7%)。在用生物质燃油时, OGT2500 基本负荷额定输出功率也是 2 670 kW。该燃气轮机的压比是 12.0: 1, 质量流量为 15.0 kg/s, 排气温度为 460 °C。

在应用生物质燃油时, 燃料喷嘴有三个通路, 以便来输送馏出油(启动时应用)、生物质燃油(正常运行时应用)、以及用于燃油雾化的燃气轮机压气机的抽气。

(吉桂明 供稿)

317~321

A numerical simulation study of a full-scale three-dimensional combustion has been conducted of a low-heat-value coal-bed gas burner along with a forecast of flow fields, temperature and constituent distribution at the outlet of the burner. Investigated also was the impact of different thermal loads and nozzle patterns on the burner performance. The results of the study show that the burner has the ability to regulate a relatively wide range of loads with the converging nozzle burner having the highest combustion temperature and a good rigidity of jet flow. The diverging nozzle burner has the optimal combustion characteristics during the thermal loads ranging from 50% to 100% and the converging nozzle burner has the optimal combustion performance at 25% thermal load. The simulation results may serve as a helpful guide for furthering the optimized design of the burner. **Key words:** low heating value, coal-bed gas burner, numerical simulation, thermal load

熔池内 Li/SF₆ 缓慢燃烧可行性的实验研究 = **An Experimental Study of the Feasibility of Li/SF₆ Slow Combustion in a Molten Pool Reactor** [刊, 汉] / LI Yan (Military Representative Office of the Naval Forces of Chinese PLA Resident at Harbin Turbine Works Co. Ltd., Harbin, China, Post Code: 150046), ZHANG Li-chao, ZHENG Hong-tao (College of Power and Energy Source under the Harbin Engineering University, Harbin, China, Post Code: 150001) // Journal of Engineering for Thermal Energy & Power. — 2007, 22(3). — 322~325

On the basis of experiments an exploratory study has been conducted of the feasibility of Li/SF₆ slow combustion in a molten pool reactor. During the three experiments separately performed, through nozzles SF₆ gas was sprayed at a pressure difference of 0.06 MPa into an air-tight molten pool reactor of 430 °C initial temperature containing liquid-state metal lithium. A slow combustion reaction between SF₆ and liquid lithium was made to occur at the liquid surface. Through a control of the flow rate of SF₆ taking part in the combustion, a preset temperature has been attained in the reactor. The preset temperatures were 500 °C, 565 °C and 780 °C respectively under which the reactor worked stably for a period of time. On the basis of the test data, an analysis was performed of the experimental phenomena. Effective measures were taken to avoid nozzle blockage during the experiments. Through the experiments it has been verified that the slow combustion of Li/SF₆ occurring at the liquid surface in the air-tight molten pool reactor can be fully controlled. Under the regulation of the control system, the temperature can reach a preset one only after a single adjustment with the maximal temperature fluctuation being within a range of ±5 °C and the pressure value being totally dependent on the temperature in the reactor. **Key words:** lithium, SF₆, molten pool reaction, slow combustion

液-液雾化的射流特性与粒径分布 = **Liquid-liquid Atomized Jet-flow Characteristics and Particle Diameter Distribution** [刊, 汉] / LIANG Kun-feng, PENG Zheng-biao, YUAN Zu-lin, et al (College of Energy Source and Environment under the Southeast University, Nanjing, China, Post Code: 210096) // Journal of Engineering for Thermal Energy & Power. — 2007, 22(3). — 326~331

The particle diameter distribution of liquid droplets is one of the key factors involved in the technology for making fluid ice from a liquid-liquid circulating fluidized bed. On a fluidized bed test device, by using a method combining high speed photography with image processing, a study has been conducted of the liquid-liquid single-hole atomized jet-flow at a low flowing speed and its impact on the distribution of particle diameters of liquid droplets. In this connection, a mathematico-statistical method was employed to analyze the change in jet flow length and the distribution of particle diameters of liquid droplets. It has been found from the analysis that a jet flow emerges when its speed is greater than 1.14 m/s and the fluctuations in the jet flow length at various flow speeds assume a random and non-periodic character. Moreover, with an increase of the jet flow speed the mean value and variance of the jet flow length show an overall variation tendency of "first increase and then decrease". With the jet flow speed being 6.58 m/s, which is a turning point, a spherical or

conical jet-flow top is formed at the peak point of the jet flow length fluctuations. This is the main reason why there emerged a difference in magnitude of the particle diameters of liquid droplets and their movement routes showed signs of wobbling. At various flow speeds, the distribution of particle diameters of the liquid droplets is in very good agreement with Rosin-Rammler distribution. The research results provide a reliable basis for controlling the distribution of particle diameters of liquid droplets resulting from atomization during the actual operation of a liquid-liquid circulating fluidized bed. **Key words:** liquid-liquid circulating fluidized bed, liquid-liquid atomization, jet flow, liquid droplet, particle diameter distribution

O₂/CO₂ 气氛下煤燃烧产物的热力学分析 = A Thermodynamic Analysis of Coal Combustion Products in O₂/CO₂ Atmosphere [刊, 汉] / LI Ying-jie, ZHAO Chang-sui, DUAN Lun-bo (Education Ministry Key Laboratory on Clean Coal Power Generation and Combustion Technology under the Southeast University, Nanjing, China, Post Code: 210096) // Journal of Engineering for Thermal Energy & Power. — 2007, 22(3). — 332 ~ 335

By using ASPEN PLUS software platform, a thermodynamic simulation calculation has been conducted of coal combustion products in O₂/CO₂ atmosphere. During the calculation, a comparison has been made of the coal combustion products in O₂/CO₂ atmosphere with those in air. A study has also been performed of the impact of the combustion temperature and excess oxygen factor φ in O₂/CO₂ atmosphere on the combustion products of coal. The results of the study show that NO_x amount produced from coal combustion in O₂/CO₂ atmosphere is far less than that produced in air. With an increase of temperature and φ , NO_x amount will increase. The temperature has a very small influence on the formation of SO₂ and SO₃ amount. When φ is less than 1, SO₂ amount will increase with an increase of φ . When φ is greater than 1, the change of φ will have little influence on the formation of SO₂ amount, and SO₃ amount will slightly increase with an increase of φ . The calculation data are basically in agreement with the test results available from current literature. This shows that using ASPEN PLUS software to simulate coal combustion in a rich oxygen atmosphere is a feasible approach. **Key words:** ASPEN PLUS, O₂/CO₂ atmosphere, coal combustion process, combustion product

CaCO₃ 换热结垢过程控制机理分析 = An Analysis of the Mechanism Governing the Control of CaCO₃ Scale Formation Process [刊, 汉] / XING Xiao-kai (Key Laboratory on Urban Oil and Gas Transmission and Distribution Technology under the China State Petroleum University, Beijing, China, Post Code: 102249), JING Dong-feng (Qinghai Oil Field No. 3 Oil Production Plant, Mangya, China, Post Code: 816400) // Journal of Engineering for Thermal Energy & Power. — 2007, 22(3). — 336 ~ 339

To gain an in-depth understanding of the mechanism involved in the control of a scale formation process, a resistance formula relating to the control of a scaling process has been identified through an analysis of CaCO₃ scale formation on heat exchange surfaces. The calculation results show that the greater the flow velocity, the lower the supersaturation degree, and the easier the scale formation process will be controlled by a surface reaction. The slower the flow velocity, the greater the supersaturation degree, and the easier the scale formation process will be controlled by convection mass transfer. Moreover, the above process tends to occur under circumstances when liquid walls have a relatively big temperature difference and a relatively high temperature. During the scale-layer growing process and under the condition of the wall temperature being a constant, the scale formation process jointly controlled by the convection mass transfer and the surface reaction may shift to one controlled only by the surface reaction. The control mechanism will remain unchanged under the condition of a constant heat flux. **Key words:** CaCO₃, scale formation, convection mass transfer, surface reaction